JOURNAL OF MAGNETIC RESONANCE **132,** 54–64 (1998)
ARTICLE NO. MN981383

Super-*Q* Detection of Transient Magnetic Resonance Signals

B. H. Suits,[1] A. N. Garroway, and J. B. Miller

Chemistry Division, Naval Research Laboratory, Washington, DC 20375-5342

Received June 5, 1997; revised November 12, 1997

The signal-to-noise ratio (SNR) improvements with increasing detection coil quality factor, *Q*, are examined for the detection of known magnetic resonance signals in noise. It is found that in the absence of amplifier noise, SNR continues to increase with increasing *Q* even in the "super-*Q*" limit, when the bandwidth of the tuned detection circuit is smaller than that of the signal to be detected. In the super-*Q* limit, the maximum obtainable SNR is thus limited by noise from the amplifiers in the system. This contrasts with typical NMR measurements where the ultimate SNR is limited by thermal noise from the detection circuit. Explicit expressions are derived and are compared to experiments performed using electronically simulated spin echo signals.

INTRODUCTION

Magnetic resonance has been found to be useful to detect quantitatively the presence of specific substances within an inhomogeneous sample. For such a measurement, the nature of the signal from the substance to be detected is known and only the strength of that signal needs to be measured. Ultimately, the minimum detectable quantity of the substance is limited by signal-to-noise considerations.

It has long been known (*1*) that the signal-to-noise ratio (SNR) of a magnetic resonance measurement can be improved by placing the sample in a tuned circuit with a high-quality factor, Q, with a typical sensitivity improvement which scales as $Q^{1/2}$. The resulting bandwidth of the tuned detection coil is then f/Q, where f is the resonant frequency of the tuned circuit. However, in the vast majority of, if not all, pulsed magnetic resonance measurements, the bandwidth of the detected signal[2] is small compared to the bandwidth of the tuned detection coil. Here we present the results of an investigation into the case where the bandwidth of the tuned detection coil is much smaller than that of the signal to be detected. We refer to this as "super-*Q*" detection. This work was inspired by comments made to us by Dr. Richard Garwin of IBM and work done to optimize acoustic sensors for the detection of gravity waves (*2, 3*). We find that

- the detection sensitivity in the super-*Q* limit continues to increase with increasing *Q* and
- the detection sensitivity is not inherently limited by the thermal noise from the detection circuit, but by noise added later in the system.

Implementation of super-*Q* detection may require a significant effort and may not be possible in some cases. Our results can be used to help determine whether that effort is warranted. The results here could have applicability to low-frequency NQR or NMR work, to broad line NMR studies such as stray field imaging of materials, and possibly to pulsed EPR spectrometers using high-*Q* cavities. We note that superconducting coils with *Q*'s of up to 100,000 have been used for NMR measurements (*4–6*).

The results here are formulated for traditional Faraday detection of NMR signals; however, they may have applicability for other high-*Q* NMR detection schemes, for example, the use of small mechanical cantilever beams such as those found in atomic force microscopes (*7*).

The study here is limited to the receiving system. In any application which will use a super-*Q* detection system for pulsed magnetic resonance, the method used to create the rf excitation and the ring-down of the detection system after that excitation also need to be considered. A traditional single coil NMR system would require the use of a very large rf power level during the excitation to achieve the high-*Q* limit discussed here. Separate excitation and detection coils, possibly with dynamic frequency shifting and/or *Q*-switching circuits, might be useful to achieve a broad band excitation with minimal interference from coil ring-down. In any case there will be a significant time interval after the excitation, the "dead time," when a signal is unobservable. Hence, it is presumed here that the observed signal is in the form of an echo with a time duration, τ, which has formed well after this dead time. That echo occurs at a known time. It is convenient to express many of the results in terms of a reduced Q, $Q' \equiv Q_L/Q_S$, the ratio of the loaded Q, Q_L

[1] To whom correspondence should be addressed. Permanent address: Physics Department, Michigan Technological University, Houghton, MI 49931-1295.

[2] Note that the bandwidth for the detected signal is the excitation bandwidth convoluted with the NMR line width.

1090-7807/98 $25.00

(defined below), of the detection system to the ''Q'' of the echo signal, $Q_S \equiv 1/f\tau$, the ratio of the bandwidth of the echo signal, $1/\tau$, to the frequency. With these definitions, super-Q detection corresponds to $Q' \gg 1$. Though the specific results here are for an echo signal, the general principles of super-Q detection can be applied to any signal which has rapid changes in amplitude which occur in a time scale, τ, and $Q_L/f\tau > 1$.

To put values of Q' in perspective, an NMR measurement of a 50-kHz-wide proton line at 500 MHz using a coil with $Q = 100$ would correspond to $Q' \approx 0.01$, an NMR measurement at 100 MHz of a severely broadened Cu spectrum (such as from a high-temperature superconductor) with an rf excitation of $B_1 = 50$ G (5 mT) using a coil with $Q = 100$ would have $Q' \approx 0.1$, and a 1-kHz-wide ^{14}N NQR line at 1 MHz detected with a coil with $Q = 100$ would also have $Q' \approx 0.1$. On the other hand, a 10-kHz-wide ^{14}N NQR line at 1 MHz using a coil with $Q = 1000$ would have $Q' \approx 10$.

First we summarize the relevant theory for computing SNR for an NMR receiver with super-Q detection in mind. The optimized (or ''matched'') filter in the presence of non-white noise is presented and used to make a fair comparison between the different cases. This is followed by a discussion of detectability for the super-Q case. Explicit expressions are derived for the changes in SNR with Q for the case of a simplified echo signal. The experimental results obtained using electronically simulated NMR spin echoes are then presented to illustrate the improvements in detectability in the super-Q limit.

THEORY

Model Circuit

Because the signal-to-noise characteristics of a detection scheme depend on the details of the probe circuit, we begin by summarizing well-known results in a useful format.

The model circuit we use is shown in Fig. 1a, where v_{th} and Z are the Thevenin equivalent voltage and impedance of the NMR probe; i_a and v_a represent current and voltage noise sources, respectively, used to model the noise from the amplifier; and A and R_a are the gain and the input impedance of the amplifier. The model resistor R_a is noiseless. The voltage in the probe, v_{th}, includes both signal and thermal noise; however, we will treat the noise separately. We assume, and later verify experimentally, that the noise from the amplifier and the noise from the probe are uncorrelated. The probe is assumed to be at a temperature T and the observed thermal noise will depend on the real part of Z (8). Straightforward analysis shows that the noise power density (in units of V^2/Hz) at the input of the amplifier, $P(\omega)$, is given by

$$P(\omega) = v_a^2 + i_a^2\left|\frac{ZR_a}{Z+R_a}\right|^2 + 4kT\,\mathrm{Re}(Z)\left|\frac{R_a}{Z+R_a}\right|^2$$

$$= P_A(\omega) + P_0(\omega), \qquad [1]$$

where P_A represents the noise which vanishes for a noiseless amplifier and P_0 is due to the thermal noise from the tuned detection circuit.

In order to obtain an expression for the signal, and explicit expressions for Z in Eq. [1], details of the particular probe circuit need to be considered. Here we consider the parallel-tuned detection circuit shown in Fig. 1b. A similar analysis with similar results can be carried out for other tuned detection circuits. The sample is contained in L. The inductor L' is used for impedance matching. Losses in L' and in the cables connecting the detection circuit are considered small compared to R_a, and the noise associated with those losses is included in the amplifier noise. For longer cable lengths,

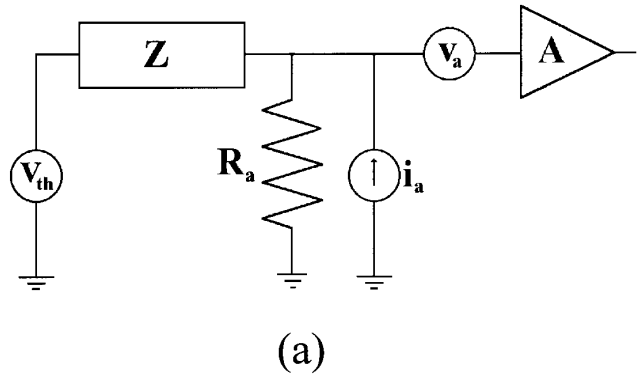

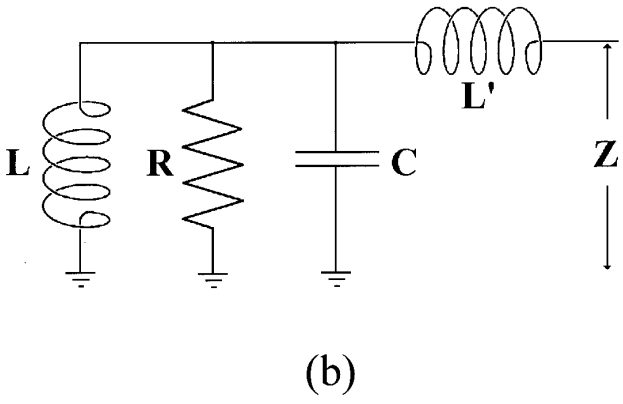

FIG. 1. (a) Model circuit for a simplified NMR receiver. The NMR probe is modeled using an impedance, Z, and the amplifier with current and voltage noise sources, a noiseless resistance, and a noiseless amplifier. (b) One type of tuned circuit which can be used as an NMR probe. The sample to be measured is placed in L. The values of L' and C are adjusted for a resonant impedance match at the desired frequency of operation.

the impedance transformation due to the cable also needs to be considered.

The values of C and L' are adjusted as needed to make the resonant circuit have a real impedance, $Z = R_0$ ($R_0 \leq R$), at a particular frequency, ω_0. This is achieved by choosing

$$C = \frac{1}{\omega_0^2 L}\left(1 + \frac{1}{Q}\sqrt{\frac{R - R_0}{R_0}}\right)$$

$$= \frac{1}{\omega_0^2 L}\left(1 + \frac{1}{Q}\sqrt{\frac{\omega_0 LQ - R_0}{R_0}}\right) \qquad [2]$$

and

$$L' = \frac{1}{\omega_0}\sqrt{R_0(R - R_0)}$$

$$= \frac{1}{\omega_0}\sqrt{R_0(\omega_0 LQ - R_0)}\,, \qquad (3)$$

where $Q \equiv R/\omega_0 L$. A similar expression is obtained if a capacitance, C', is used for impedance matching instead of an inductance. Using Eqs. [2] and [3], it is found that

$$Z = i\omega LR^2\left[\frac{\omega_0^2 LC - 1}{[R(\omega_0^2 LC - 1)]^2 + \omega_0^2 L^2}\right.$$

$$\left. - \frac{\omega^2 LC - 1}{[R(\omega^2 LC - 1)]^2 + \omega^2 L^2}\right]$$

$$+ \frac{\omega^2 L^2 R}{[R(\omega^2 LC - 1)]^2 + \omega^2 L^2} \qquad [4]$$

and when ω is near ω_0, this can be approximated quite well by the simpler expression

$$Z = i\omega L\left[\frac{\omega_0^2 LC - 1}{[(\omega_0^2 LC - 1)]^2 + \frac{1}{Q^2}}\right.$$

$$\left. - \frac{\omega^2 LC - 1}{[(\omega^2 LC - 1)]^2 + \frac{1}{Q^2}}\right]$$

$$+ \frac{R/Q^2}{[(\omega^2 LC - 1)]^2 + \frac{1}{Q^2}}\,. \qquad [5]$$

The nuclear magnetization will induce an EMF in L due to the time changing magnetic flux, $\phi(t)$. In the frequency domain, this gives rise to a Thevenin equivalent voltage source for the desired signal,

$$v_{\text{th}}(\omega) = i\omega\phi(\omega)\,\frac{1}{(1 - \omega^2 LC) - i\omega L/R}$$

$$\approx i\omega\phi(\omega)\,\frac{1}{(1 - \omega^2 LC) - \dfrac{\mathrm{i}}{Q}}\,. \qquad [6]$$

So the signal, $S(\omega)$, at the input of the amplifier will be

$$S(\omega) = v_{\text{th}}(\omega)\,\frac{R_{\text{a}}}{Z(\omega) + R_{\text{a}}}\,. \qquad [7]$$

When $Q\omega_0 L \gg R_0$, and with the assumption $R_{\text{a}} \lesssim \omega_0 L$, Eq. [7] can be approximated by

$$S(\omega) = i\omega\phi(\omega)\left[\frac{-iR_{\text{a}}(QR_0\omega_0 L)^{-1/2}}{(\omega^2 - \omega_0^2)LC - \dfrac{i}{Q}\left(\dfrac{R_0 + R_a}{R_0}\right)}\right]$$

$$\times\left[\frac{\omega^2 LC - 1 - i/Q}{\omega^2 LC - 1 + i/Q}\right]. \qquad [8]$$

The approximation is valid when $\omega \approx \omega_0$; $S(-\omega) = S^*(\omega)$ is used when $\omega \approx -\omega_0$.

At first sight, Eq. [8] would suggest a net loss in SNR for super-Q detection since only the nuclear signals within a narrow bandwidth around ω_0 will be detected. However, as we show below, there may be a substantial gain. To some extent, such gain can be compared to an analogous pulsed magnetic resonance measurement, but employing the nuclei as the detector of pulsed rf. In this case, the best signal-to-noise ratio is achieved for nuclei with long relaxation times (T_2 in this case) compared to the rf pulse length, even though the nuclei only ''see'' the component of the pulsed rf at their resonant frequency.

Some additional insight can be obtained by transforming Eq. [8] into the time domain. The details of the result depend, of course, on the shape of $\phi(\omega)$. As an example, consider the simple case where $\phi(t)$ is a square pulse of frequency ω_0 and duration τ, starting at a time $t = -\tau$. Then the signal, $s(t)$, is given to a good approximation by

$$\begin{aligned} s(t) &= 0 && t < -\tau \\ s(t) &= A\sqrt{T_Q}(1 - e^{-(t+\tau)/T_Q})e^{i\omega_0 t} && -\tau < t < 0 \\ s(t) &= A\sqrt{T_Q}(1 - e^{-\tau/T_Q})e^{i\omega_0 t}e^{-t/T_Q} && t > 0, \end{aligned} \qquad [9]$$

where $T_Q \equiv 2Q_{\text{L}}/\omega_0$ is the rise time of the tuned detection circuit; Q_{L} is the ''loaded Q'' of the detector coil, $Q_{\text{L}} = R_0 Q/(R_0 + R_{\text{a}})$, and A is an overall amplitude proportional to the amount of sample present. Super-Q detection corresponds to the case where $\tau \ll T_Q$ while conventional SNR calculations are done for the case $\tau \gg T_Q$. Hence, the time-

dependent exponential rise of the signal during the interval $-\tau < t < 0$ (that is, the transient response of the detection coil) will be very important for super-Q detection while only the steady state value is needed for the calculations in the conventional case. When $\tau \ll T_Q$ the maximum signal height will be significantly less than its steady state value and one can conclude quite correctly that the peak height of the signal for super-Q detection is less than that for the conventional case. It will be shown below, however, that SNR for signal detection actually increases.

There are two important time scales evident for super-Q detection. The rise of the signal occurs over the time τ, and the decay of the signal over the (longer) time T_Q.

Note that for traditional magnetic resonance measurements, the signal from the coil follows the excitation (i.e., $S(\omega) \propto i\omega\phi(\omega)$), and no distinction is usually made between the coil response and the EMF due to the precessing nuclear magnetization. However, in the super-Q limit, the coil response *does not* follow the NMR magnetization. Unless specifically qualified, we use the word ''signal'' in what follows to mean the measured response of the coil due to excitation by the nuclear magnetization.

In order to calculate SNR, the noise from the tuned detection circuit, P_0, and from the amplifier, P_A, need to be carefully considered as well. Neglecting the noise from the amplifier for the moment, and noting that

$$\mathrm{Re}(Z) = \left| \frac{\sqrt{R}/Q}{(1 - \omega^2 LC) + \dfrac{i}{Q}} \right|^2, \qquad [10]$$

we find that the noise power density from the tuned probe is given by

$$P_0(\omega) = \frac{4kT\omega_0 L}{Q} \left| \frac{S(\omega)}{i\omega\phi(\omega)} \right|^2 \qquad [11]$$

and $P_0(\omega_0) = 4kTR_0[R_a^2/(R_a + R_0)^2]$, as expected. When the NMR signal is narrow compared to the probe bandwidth, this noise is, for all practical purposes, white noise.

As will be seen below, Eq. [11] is the important result for super-Q detection, as it shows the direct relationship between the amplitude of the thermal noise from the probe and the amplitude of the received signal.

Optimized Filter

Typically the SNR is determined by comparing the signal height (in either the frequency or the time domain) to the root mean square (RMS) noise. The more general question is, ''How do we combine the measured data points in the best possible way to determine the amount of signal present and how does that compare to the noise?'' Conventional NMR methods will use bandpass filters, Fourier transforms, apodization, and similar techniques to help make the desired signal stand out against the noise. It is worth pointing out that none of these techniques increases the information content of the measured signal, and in fact they may decrease it.

In order to make a fair comparison between the SNR obtainable in different circumstances, we make use of a linear optimized filter. SNR here is a measure of our ability to determine one number, the amplitude of a known signal in noise, using an appropriate combination of all the data acquired. Hence this analysis is not directly applicable for the measurement of unknown NMR spectra.

As is well known (*9–11*), the SNR in the presence of stationary white noise can be maximized at a particular time[3] after the signal, t_m, by applying a matched filter, $H(\omega)$, where

$$H(\omega) = S^*(\omega)e^{-i\omega t_m} \qquad [12]$$

and $S^*(\omega)$ is the Fourier transform of the known desired signal. When the noise is not white, the matched filter can be preceded by a whitening filter, $H'(\omega)$, satisfying

$$|H'(\omega)|^2 P(\omega) = |C|^2, \qquad [13]$$

where C is any constant and $P(\omega)$ is the noise power density (*10*). With (noncausal) postprocessing, we are free to choose $H'(\omega)$ to be real, $C = 1$, and $t_m = 0$ for convenience. The signal after the filters is given by

$$\begin{aligned} s_0(t) &= \frac{1}{2\pi}\int_{-\infty}^{+\infty} S(\omega)H'(\omega)H(\omega)e^{i\omega t}d\omega \\ &= \frac{1}{2\pi}\int_{-\infty}^{+\infty} CS(\omega)P(\omega)^{-1/2}H(\omega)e^{i\omega t}d\omega \end{aligned} \qquad [14]$$

and the noise by

$$\langle n_0^2(t)\rangle = \frac{1}{2\pi}\int_{-\infty}^{+\infty} |C|^2|H(\omega)|^2 d\omega. \qquad [15]$$

The derivation of the matched filter using the Schwartz inequality proceeds as in the case of white noise (*9, 10*) to give an optimized filter

$$H(\omega) = S^*(\omega)P(\omega)^{-1/2}e^{-i\omega t_m} \qquad [16]$$

and an optimized SNR at a time t_m given by

[3] The time, t_m, is important for the design of a physically realizable filter and expresses the fact that for a physically realizable filter, the maximum SNR will occur at a time after the excitation has occurred. If the filter is implemented using numerical postprocessing, as we do in this work, one can set $t_m = 0$.

$$(\mathrm{SNR})^2 = \frac{s_0^2(t_m)}{\langle n_0^2(t)\rangle} = \frac{1}{2\pi}\int_{-\infty}^{+\infty} \frac{|S(\omega)|^2}{P(\omega)}\, d\omega. \quad [17]$$

Since no initial assumptions were made regarding $H(\omega)$, Eq. [17] gives the best SNR obtainable with a linear filter. This filter can be implemented in hardware using standard rf filters and/or during postprocessing of acquired data. Since the filter is likely to be realized only approximately using hardware, and it is undesirable to modify the hardware for each new circumstance, postprocessing will generally be more convenient. The application of optimized filters to finite discrete data is discussed in Ref. (*10*). We also note that an optimized filter can be derived in the time domain resulting in the same value for the SNR as above.

In the super-Q limit, $Q' \gg 1$, the excitation from the nuclei and the noise from the probe, referenced to the coil, L, are both broadband and both enter the circuit at the same point. If an ideal amplifier with a noise figure (NF) of 0 dB is used, then $P(\omega) = P_0(\omega) \propto |S(\omega)|^2$. That is, the SNR is independent of frequency. Hence, by averaging together all the frequency components with appropriate weights, the combined SNR tends to infinity with increasing Q' *even though the detection coil is at a finite temperature.* In this limit, the amplitude of thermal noise from the detection system is not, by itself, an inherent limit to signal detection. In practice, the finite duration of the excitation (making the bandwidth of $S(\omega)$ less than that of $P(\omega)$) and the amplifier noise (which causes SNR to decrease with decreasing $|S(\omega)|$, rather than SNR remaining constant) conspire to keep SNR finite.

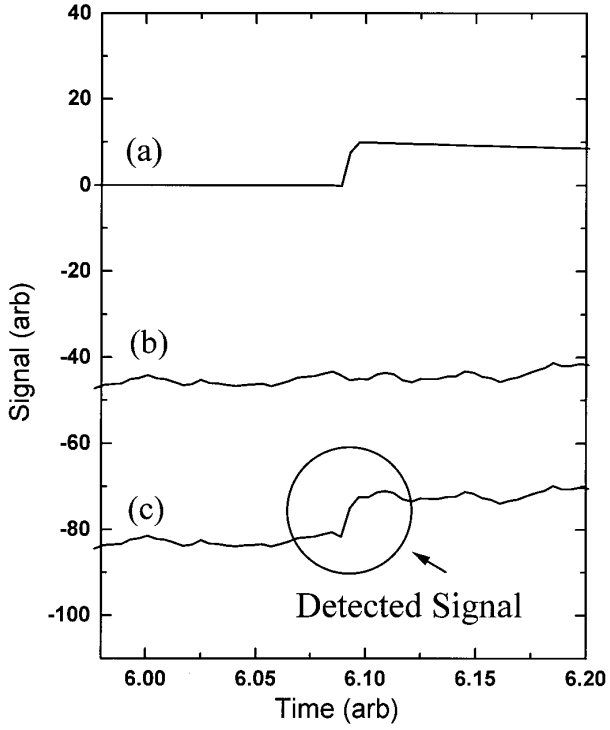

FIG. 3. The same data as Fig. 2, but on a much expanded time scale. The signal is clearly observable in (c) even though the RMS noise level is much larger than the signal height.

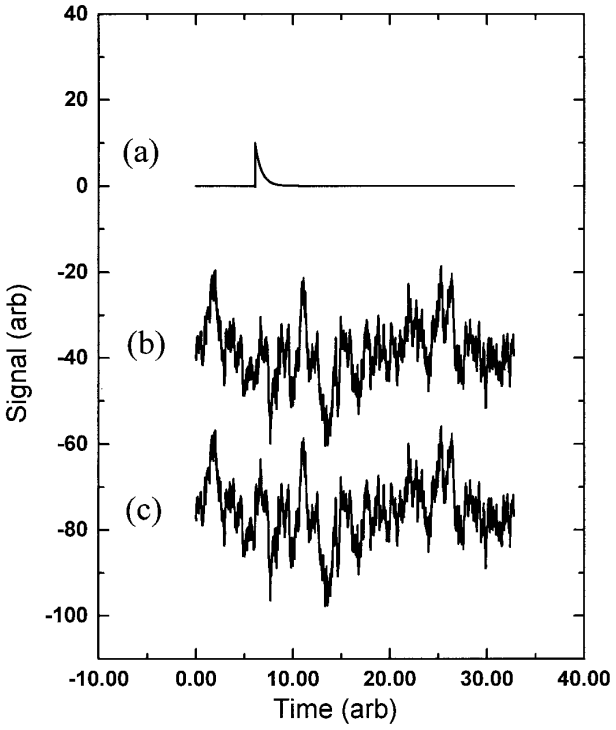

FIG. 2. Numerical simulations of super-Q measurements made with a perfect amplifier. (a) A signal in the absence of noise, (b) thermal noise from the probe, and (c) the sum of (a) and (b).

Detectability

First we illustrate the essence of super-Q detection by considering the case where amplifier noise is negligible. Figure 2 shows three possible measurements, simulated numerically. Figure 2a shows the Fourier transform of a (complex) Lorentzian lineshape and represents the envelope of the tuned coil response to a short excitation in the absence of noise. Figure 2b is the Fourier transform of the same Lorentzian lineshape, though with 10 times greater amplitude and with the phase of each frequency component randomized. Figure 2b represents the envelope of thermal noise from the tuned coil. Hence $|S(\omega)|^2$ has the same shape for both the signal and the noise, and the desired signal in Fig. 2a is reduced by 20 dB compared to the noise. Figure 2c is the sum of the data in Fig. 2a and 2b. If SNR is defined in the time domain using the peak signal height compared to the RMS noise, then clearly SNR < 1. However, because the thermal noise from the tuned circuit is not white, this signal is easily detected with SNR > 10, as is illustrated in Fig. 3. Figure 3 contains the same data as does Fig. 2, except

on an expanded time scale. Clearly the desired detection scheme, and the resulting definition of SNR, might be improved if one looks for the rapid rise of the signal over the time, τ, of the excitation. The rapid rise of the signal compared to what is seen in the noise occurs due to the correlations between the phases of the frequency components of the signal and is not due to the correlations in their amplitudes. The probability that such an alignment of the phases (of the frequency components of the noise) would occur by accident is very small. The probability that such an alignment would occur in just the right way so that an apparent signal shows up just at the right time is even smaller.

The weighting of the measured data to bring out this rapid change would correspond to a high pass filter. Recognizing that the data in Figs. 2 and 3 are the envelopes which modulate a carrier signal at ω_0, we see that the high pass filter corresponds to a notch filter with a notch at ω_0. Application of a notch filter at the signal frequency in order to improve the SNR may, at first, seem counterintuitive, but can be better appreciated by the following argument.

An estimate of the SNR can be obtained by considering an experiment which measures the difference between two measured data points, one just before the excitation is expected and one just after. If the excitation starts just after time t and is finished at a time $t + \tau$, the SNR for this crude measurement scheme will be given by

$$(\mathrm{SNR})^2 = \left\langle \left(\frac{s(t+\tau) - s(t)}{n(t+\tau) - n(t)} \right)^2 \right\rangle$$

$$= \frac{s^2(t+\tau)}{2\langle n^2(0)\rangle \left(1 - \dfrac{\langle n(\tau) n(0)\rangle}{\langle n^2(0)\rangle} \right)}. \qquad [18]$$

In the absence of amplifier noise, this is

$$(\mathrm{SNR})^2 = \frac{s^2(t+\tau)}{2\langle n^2(0)\rangle (1 - e^{-\tau\pi f/Q_\mathrm{L}})} \qquad [19]$$

and since $s^2(t+\tau) \propto 1/Q_\mathrm{L}$ and $\langle n^2(0)\rangle \propto 1/Q_\mathrm{L}$, then in the super-$Q$ limit, SNR $\propto Q_\mathrm{L}^{1/2}$.

Now we consider super-Q detection for the case where the amplifier noise dominates the signal. For this illustration we model the amplifier using (broad band) white noise. Since the noise at $t + \tau$ is uncorrelated with the noise at t, the two-point detection scheme above gives $(\mathrm{SNR})^2 = s(t + \tau)^2/2\langle n^2(0)\rangle$ and SNR $\propto Q_\mathrm{L}^0$. In this case, it would be more convenient to take advantage of the long ring-down time, T_Q, and to look for a narrow line in the frequency domain. For a narrow line in the frequency domain one measures $(S(\omega_0) - S(\omega_0 \pm \Delta\omega))$ where $\Delta\omega \gtrsim \omega_0/Q_\mathrm{L}$. For such a measurement one would use a bandpass filter identical

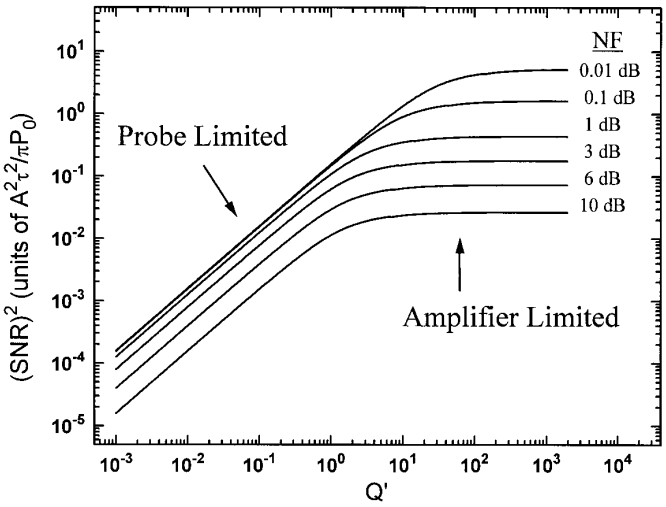

FIG. 4. The signal-to-noise ratio after a square pulse excitation and with a white noise approximation for the amplifier, from Eq. [21].

to optimal detection in conventional NMR except that the line width here is determined by the filtering action of the detection circuit. The optimum SNR $\propto Q_\mathrm{L}^0$ here as well.

The actual case will look something like a combination of the two limiting cases discussed above and the optimum filter will look like a bandpass filter with a notch in the middle. The depth of the notch and the width of the bandpass will be determined by the relative sizes of the amplifier and probe noise. The optimized filter computed as discussed above automatically has these characteristics.

In order to explicitly illustrate the effectiveness of super-Q detection we consider the response of the tuned detection circuit to a square excitation at a frequency ω_0 and of duration τ as given by Eq. [9]. Obtaining $S(\omega)$ from Eq. [9] is straightforward.

The noise power density will then be given by

$$P(\omega) = P_0 \frac{1/T_Q^2}{(\omega - \omega_0)^2 + 1/T_Q^2} + P_\mathrm{A}(\omega), \qquad [20]$$

where $P_0 = P_0(\omega_0)$ is the peak thermal noise power density from the tuned and matched detection circuit, and P_A represents the additional noise from the amplifier. To keep matters simple at this point, it is assumed that P_A is a constant, though a more detailed analysis should include the frequency dependence of P_A, which in turn depends on the particular hardware used. In the white noise case, the minimum noise figure, NF, occurs at ω_0 and is given by NF $\equiv (P_0 + P_\mathrm{A})/P_0$, often expressed in dB. The signal-to-noise ratio after the application of the optimized filter can be calculated using Eq. [17] to be

$$(\mathrm{SNR})^2 = \frac{1}{2\pi^2}\frac{A^2\tau^2 Q'}{P_A + P_0}\left[1 - \frac{Q'}{b}(1 - e^{-b/Q'})\right], \quad [21]$$

where it is recognized that $T_Q/\tau = Q'/\pi$ and

$$b = \pi\sqrt{\frac{P_A + P_0}{P_A}}. \quad [22]$$

Figure 4 illustrates the changes in SNR as a function of Q' determined using Eq. [21] for a variety of values of NF. As can be seen, for $Q' < 1$, there is little improvement in SNR as NF is decreased below 1 dB. However, when $Q' \gg 1$, there is still a significant improvement as NF is decreased. The SNR in Fig. 4 is in units of

$$\frac{A^2\tau^2}{\pi P_0} = \left[\left|\frac{d\phi}{dt}\right|^2 \frac{\tau}{\omega_0 L}\right]\left[\frac{1}{4kT}\right]\left[\frac{\omega_0\tau}{2\pi}\right]$$

$$= \frac{1}{8\pi}\left|\frac{d\phi}{dt}\right|^2 \frac{\tau^2}{kTL}, \quad [23]$$

where $d\phi/dt$ represents the EMF induced in the coil, L, by the nuclear magnetization during the time τ. The brackets in the first form of Eq. [23] divide the equation into terms associated with the energy delivered to the coil by the nuclear magnetization during the time τ, the thermal energy in the coil, and a scale factor which relates Q' to Q_L for the specific measurement conditions. The presence of the scale factor means that reducing τ (for example by applying a magnetic field gradient) as a way to increase Q' is *not* a good strategy for increasing SNR. Note that with all other factors held constant, $|d\phi/dt| \propto L^{1/2}$ so SNR does not depend directly on L.

In the limiting cases where $Q' \ll b$ and $Q' \gg b$, SNR is given by

$$(\mathrm{SNR})^2 = \left[\left|\frac{d\phi}{dt}\right|^2 \frac{\tau}{\omega_0 L}\right]\left[\frac{1}{4kT}\right]\frac{Q_L}{2\pi \mathrm{NF}} \quad Q' \ll b$$

$$= \frac{1}{4}\left[\left|\frac{d\phi}{dt}\right|^2 \frac{\tau}{\omega_0 L}\right]\left[\frac{1}{4kT}\right]\left[\frac{\omega_0\tau}{2\pi}\right]$$

$$\times \sqrt{\frac{1}{\mathrm{NF}(\mathrm{NF} - 1)}} \quad Q' \gg b. \quad [24]$$

These two equations are very similar in form if one equates $\omega_0\tau/2\pi$ with the ''Q of the excitation.'' The specific results (Eqs. [23] and [24]) are derived for a square excitation of length τ using a white noise model for the amplifier and illustrate the general behavior expected. For the general case, changes of order unity in the numerical factors can be expected.

Impedance Matching

The probe impedance, R_0, can be adjusted over the range $0 < R_0 < R$ by a suitable choice of L'. In the super-Q limit it is not at all obvious which value will give the best signal-to-noise ratio. In principle, the model equations above (Eqs. [1], [4], [7], [11], [17]) can be used to determine a best value for R_0 in a given situation; however, detailed discussion of this issue is deferred until a later time. Since most of the signal occurs at frequencies where the probe impedance is not R_0, specific noise characteristics of the amplifier, especially when it is not properly matched, need to be considered in order to choose the best value for R_0. In addition, the loaded Q depends on the choice of R_0 as well, and will affect correlation times and the measured signal energy. It is, however, reasonable to assume that adjusting R_0 to obtain the best amplifier noise figure at (or near) the peak of the signal, $S(\omega)$, would be a good strategy.

EXPERIMENTAL

Measurements presented here were made using a large, single-turn, open-ended copper coil designed and previously used (*12*) for ^{14}N NQR of large samples. The coil has a rectangular cross section and is 69 cm high, 43 cm wide, and 90 cm in length. Parallel capacitance is added using an arrangement of large copper sheets on the exterior of the coil and in parallel with one of the faces. The copper sheets are insulated with a thin layer of Teflon sheet. The coil is encased in a rectangular, copper-lined conducting shield with inside dimensions 0.93 m wide, 1.40 m high, and 1.83 m long. The conducting shield is closed on the ends with rf-tight doors originally designed for MRI applications. Signals are brought into and out of the shield using coaxial connectors mounted on the shield. The resulting parallel resonance frequency is 3.4 MHz with an unloaded Q of 1280. Lower values of Q were obtained by placing a carbon resistor in parallel with the coil (1 and 3 kΩ for unloaded Q's of 140 and 420, respectively). The detection system was matched to 50 Ω at resonance using the circuit shown in Fig. 2.

Impedance and Q measurements were made using an HP4195A Network/Impedance analyzer.[4] The Q measurements were made using two small, broad band magnetic field probes placed about one-third of the distance into the coil, from opposite ends. With this arrangement, the predominant coupling between the probes is through the main rf coil. Swept rf is fed into one of the probes and the received signal from the other probe is monitored as a function of

[4] Reference to a particular product is for identification only. Other products from other vendors may be suitable.

frequency. Q and Q_L are determined using the full 3-dB bandwidth of the received signal with the coil unattached and attached to the amplifier, respectively. Unless stated otherwise, 50-Ω rf components and cables are used throughout. To obtain the probe impedance data over a wide frequency range, but with sufficient resolution near the probe resonant frequency, fine measurements near resonance and coarse measurements over a wide frequency range were made and the results interleaved.

Received signals from the large coil are first amplified by a broad band Doty LN-2XL preamplifier with a nominal gain of 40 dB, nominal NF of 1.0 dB with a 50 Ω source, and a measured input impedance of 90 Ω at 3.4 MHz. A second stage of amplification is provided by an Anzac AM-110 rf amplifier with a nominal gain of 30 dB and nominal NF at 3.4 MHz of 4.2 dB. The signal is then filtered using separate 200-kHz high pass and 5-MHz low pass (RLC Electronics) filters. The signal is monitored directly and recorded using a Tektronix TDS5241A digital oscilloscope limited to a 20-MHz bandwidth. Measured signals were transferred to a personal computer for analysis and processing. The overall system gain was measured to be 68 dB at 3.4 MHz. A system NF of 1.2 ± 0.2 dB was determined from measurements of the RMS noise voltage with a 50-Ω load at room temperature and the same load immersed in liquid nitrogen.

Simulated spin–echo signals are generated using a Stanford Research Systems DS345 signal generator, a PTS-160 frequency synthesizer, a Mini-Circuits ZAY-3 mixer, and an rf attenuator. The DS345 is used in ''arbitrary waveform mode'' and is programmed with a gaussian shape approximated using 23 nonzero points and a number of zeros on either side of the gaussian. With the mixer, the rf output of the PTS-160 is amplitude modulated by the approximate gaussian waveform. The triggering was adjusted to be in phase with the rf carrier. The output from the mixer is fed through the attenuator to a small magnetic field probe (about 1 cm in diameter) placed inside the resonant coil. A small dc level adjustment (a few mV) on the output of the DS345 was necessary to minimize feedthrough of the carrier signal. When minimized, carrier feedthrough was well below the noise level. For noise measurements, the rf source was disconnected and either turned off or adjusted to a much higher frequency to avoid any possible rf leakage. For simulated spin–echo measurements, the attenuator was used to adjust the signal level and 15,000 data points (zero filled to 16,384) were measured at 50 MS/s.

Results and Discussion

Using short duration simulated spin–echoes with a gaussian shape, we measured signals for a variety of spin–echo widths for several detection coil Q's. An example of the results is shown in Fig. 5. Qualitatively one can see that the peak intensity scales roughly as $Q^{-1/2}$ when $Q' \gg 1$ and the ring-down time as Q^1, as predicted.

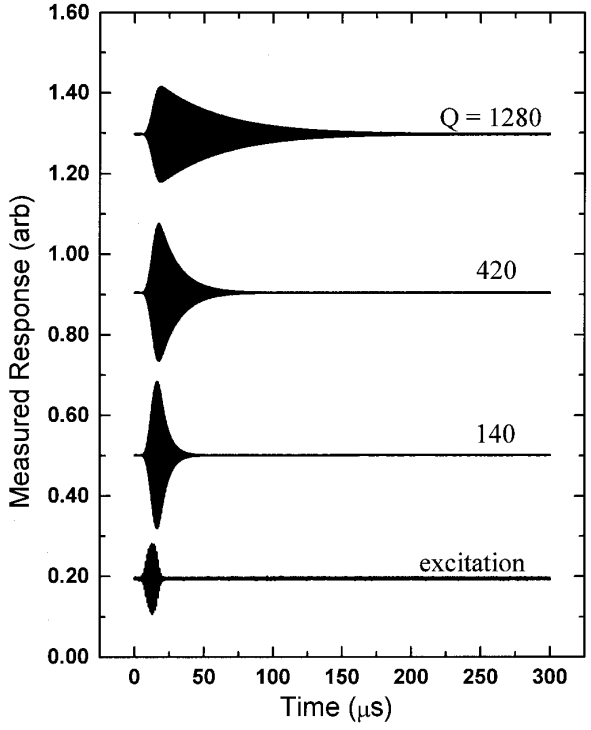

FIG. 5. Measurements of experimentally simulated spin–echoes detected in the super-Q limit. The labels on the signals correspond to the unloaded Q of the tuned detection coil. From top to bottom these correspond to $Q' = 18$, 5.5, and 2.2, respectively.

Measurements of system noise were made with a variety of amplifier loads, including the tuned and matched coil with different Q's. The noise power density was calculated using a Fourier transform of the covariance. With a sampling interval of 40 ns, a total of $N = 50{,}000$ noise measurements, $d(i)$, were made. From these, the covariance was estimated using

$$R(m) = \frac{1}{N-m} \sum_{j=1}^{N-m} d(j)d(j+m), \qquad [25]$$

where $0 \leq m \leq M$, with $M = 16{,}383$. This was repeated 40 times and the average $R(m)$ was computed. The resulting average was Fourier transformed to obtain the power spectrum. The power spectra reported here are presented in units of V^2/Hz and correspond to voltage measurements made after amplification. Measurements with a 50-Ω load, a 1-kΩ load, and a 4.7-kΩ load on the input of the amplifier were used to determine approximate amplifier noise parameters,

$$A^2 i_a^2 = 1.6 \times 10^{-4} (\mu A)^2/Hz$$
$$A^2 v_a^2 = 0.65 (\mu V)^2/Hz, \qquad [26]$$

where A is the overall gain (68 dB). A small frequency dependence has been ignored.

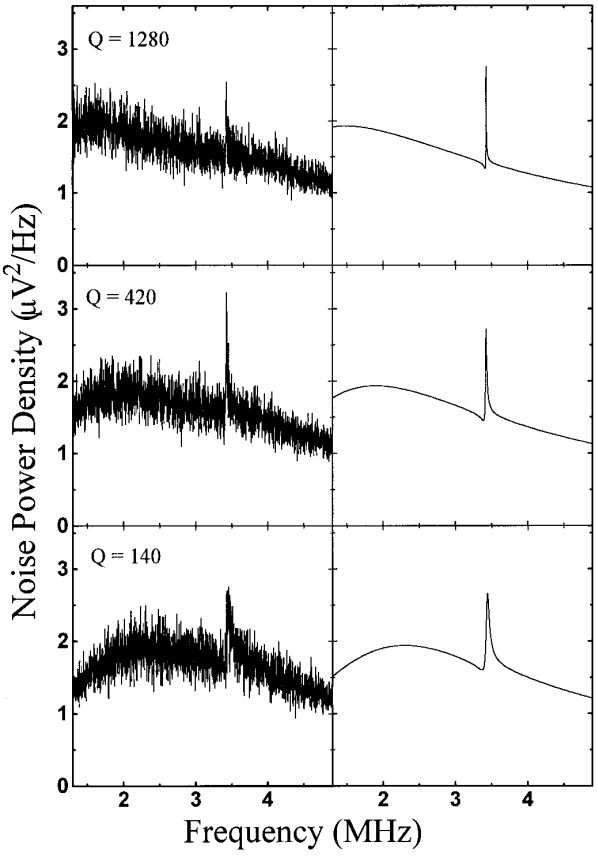

FIG. 6. Measured noise power densities for different probe quality factors, compared to values calculated from the circuit model, the two amplifier noise parameters, and the measured probe impedance.

Figure 6 shows the measured noise power density for the detection circuit, along with predictions made using Eq. [1] and the measured impedance of the detection circuit. Note that the simple two-parameter model (i_a, v_a and Eq. [1]) is adequate to fit the data with no adjustable parameters. The fact that the predictions are quite accurate shows that, as assumed above, the thermal noise from the detection circuit and the noise from the amplifier are uncorrelated. Figure 7 illustrates one of these predictions where the noise associated with the detection coil and with the amplifier have been separately identified.

By Fourier transforming a strong received signal after a very short duration simulated echo, it was verified that $|S(\omega)|^2 \propto P(\omega)$ when i_a and v_a are set to zero. The peak noise from each of the measurements of the tuned detection circuit is, within the scatter of the points, the same as that obtained by replacing the tuned circuit with a room temperature 50-Ω resistor.

As an aside, Fig. 7 also illustrates why, in this case, the detection coil should be matched to 50 Ω, even though the input to this particular amplifier has an impedance of 90 Ω. With the definition of the ''noise resistance,'' $R_n = v_a/i_a$, the value of R_0 which minimizes NF, determined using Eq. [1], is given by

$$R_0^2 = \frac{R_a^2 R_n^2}{R_a^2 + R_n^2}. \qquad [27]$$

With the measured values above, the smallest NF is predicted to occur when $R_0 = 52\ \Omega$.

The amplifier impedance has an impact on the loaded Q, Q_L, of the tuned circuit as well and hence may increase (or decrease) the SNR. For example, for our simplified circuit, Q' may be increased by about 40% by inserting a $\frac{1}{4}$-wavelength 50-Ω cable between the detection circuit and the amplifier. The loaded Q will also be an important factor determining the recovery time of the amplifier chain after excitation, and techniques such as ''overcoupling'' can be used to reduce this recovery time (*13*).

To test detection sensitivity, a ''known'' signal was measured (shown in Fig. 5) and the probe impedance as a function of frequency was recorded for each of the different Q's. In this case the width of the gaussian is $\tau \approx 8\ \mu$s corresponding to values of $Q' = 18$, 5.5, and 2.2. The known signal exceeded the noise level by more than 20 dB and was signal averaged 128 times. The excitation amplitude for the known signal was the same for each of the different values of Q. The average noise power density, $P(\omega)$, is calculated using the measured probe impedance and Eq. [1]. The known signal and the average noise power density are combined, as described above, to obtain the optimum filter. To illustrate the improved ability to detect a weak signal in the presence of noise in the super-Q regime, a sequence of measurements with reduced excitation were then recorded, without signal averaging.

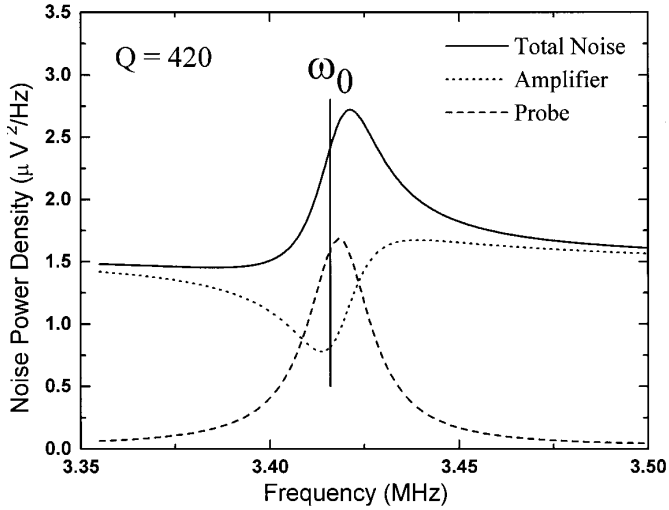

FIG. 7. The calculated values for one of the cases in Fig. 6 separated into noise power densities associated with the probe and with the amplifier.

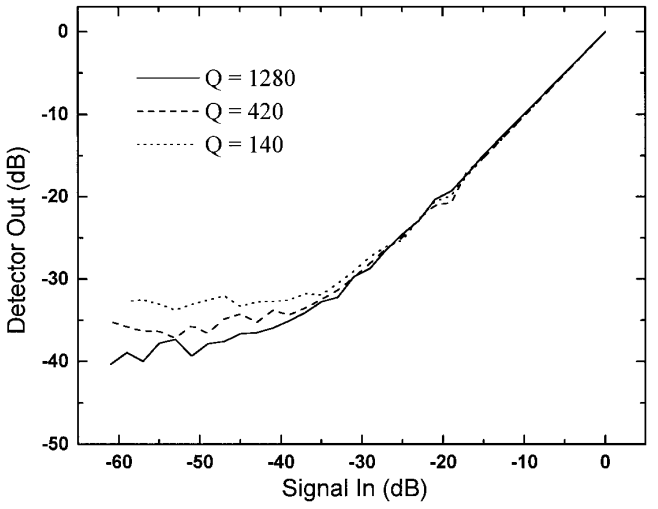

FIG. 8. Experimental detector output vs excitation for the three different values of Q. In each case, the detector output has been scaled to 0 dB for a unit (0 dB) excitation.

The digitized data are Fourier transformed and the filter is applied. The detector output is then calculated using the integral of the complex absolute value of the filtered signal. In this way, the peak of the signal envelope can be calculated simply and without the need to worry about heterodyning and overall phase shifts. That is, if $s(\omega)$ and $S_0(\omega)$ represent the Fourier transforms of the unknown signal (plus noise) and known signals, respectively, then the detector output, D, is given by

$$D = \int_{-\infty}^{+\infty} \left| \frac{s(\omega) S_0^*(\omega)}{P(\omega)} \right| d\omega. \qquad [28]$$

In practice, of course, D is calculated using discrete Fourier transforms and a summation, and $P(\omega)$ is extrapolated onto the same frequency grid as that of the signals.

Figure 8 shows the detector output, D, as a function of the amplitude of the excitation. The detector output for detection of the known signal is scaled to be 1 (0 dB) in all cases. Scaling does not change the signal-to-noise ratio, of course, and allows for easier comparison between the different cases. The flat regions on the left of Fig. 8 show that the noise level (relative to the fixed excitation used for the known signals) decreases with increasing Q. The noise level determines the size of the minimum detectable signal. While a detailed comparison of these experimental data to the predictions shown in Fig. 4, specifically that SNR improves as $Q^{1/2}$ in the super-Q regime in the absence of amplifier noise, cannot be made with the amplifier used here, we certainly see an improved SNR with an increase in detector Q in the super-Q regime and the increases are similar to those of the corresponding curves (NF = 1 to 3 dB) shown in Fig. 4.

As a final note, radiation damping may be a concern when very high-Q detection circuits are used. The effects of radiation damping for conventional detection ($Q' < 1$) are well understood (*14, 15*). For the conventional case the steady state response of the detection coil in the presence of the EMF induced by the nuclear magnetization is considered. In contrast, for super-Q detection, the transient response of the detection circuit will be important. For super-Q detection, the total energy delivered to the coil during the time τ becomes independent of Q, and that energy is ultimately dissipated over the longer time T_Q. During the time T_Q the nuclei experience the rf field produced by the transient decay of the detection coil and this could have a significant effect if one were, for example, to refocus the echo at a later time. However, the extra effort to implement super-Q detection would be undertaken only when signal levels are very small, and hence the amplitude of the transient rf field will be negligible in practice.

CONCLUSION

The signal-to-noise ratio improvements with increasing detection circuit quality factor, Q, have been examined for detecting known signals in noise. It is found that in the absence of amplifier noise, SNR continues to increase with increasing Q even in the super-Q limit, where the bandwidth of the tuned detection circuit is smaller than that of the signal to be detected. In the super-Q limit, the maximum obtainable SNR will be limited by noise from the amplifiers in the system. This contrasts with typical NMR measurements where the ultimate SNR is limited by thermal noise from the detection circuit. Explicit expressions have been derived and compared to experiments performed using electronically simulated spin–echo signals.

ACKNOWLEDGMENTS

This work is supported in part by the Federal Aviation Administration, the Office of Special Technology (Department of Defense), and the Defense Advanced Research Projects Agency. B.H.S. is a sabbatical visitor at NRL under the NRL–American Society for Engineering Education (ASEE) program.

REFERENCES

1. A. Abragam, ''The Principles of Nuclear Magnetism,'' Clarendon Press, Oxford (1961).
2. see M. J. Buckingham, ''Noise in Electronic Devices and Systems,'' Chap. 13, and references therein, Ellis Horwood, Chichester, UK (1983).
3. J. L. Levine and R. L. Garwin, *in* ''Proceedings of the 2nd ISPRA Nuclear Electronics Symposium,'' Stresa, Italy (1975).
4. Y. Kondo, J. H. Kolvuniemi, J. J. Ruohio, V. M. Ruutu, and M. Krusius, *Czech. J. Phys.* **46,** 2843 (1996).
5. R. D. Black, T. A. Early, P. B. Roemer, O. M. Mueller, A. Mogro-

Campero, L. G. Turner, and G. A. Johnson, *Science* **259,** 793–795 (1993).

6. R. D. Black, T. A. Early, and G. A. Johnson, *J. Magn. Reson. A* **113,** 74–80 (1995).
7. J. A. Sidles, *Appl. Phys. Lett.* **58,** 2854 (1991).
8. see, for example, D. A. Bell, ''Electrical Noise,'' p. 53, Van Nostrand, London (1960).
9. D. C. Champeney, ''Fourier Transforms and Their Physical Applications,'' Academic Press, New York (1973).
10. R. N. McDonough and A. D. Whalen, ''Detection of Signals in Noise,'' 2nd ed., Academic Press, San Diego (1995).
11. R. R. Ernst and W. A. Anderson, *Rev. Sci. Instrum.* **37,** 93 (1966).
12. A. N. Garroway, M. L. Buess, J. P. Yesinowski, J. B. Miller, and R. A. Krauss, *in* ''SPIE Conference Proceedings,'' Vol. 2276, pp. 139–149 (1994).
13. G. C. Chingas, *J. Magn. Reson.* **54,** 153 (1983).
14. M. Bloembergen and R. V. Pound, *Phys. Rev.* **95,** 8 (1954).
15. W. S. Warren, S. L. Hammes, and J. L. Bates, *J. Chem. Phys.* **91,** 5895 (1989).